TEMPERATURE AND WATER VAPOR RAMAN LIDAR FOR OBSERVATION OF LAND-ATMOSPHERE INTERACTIONS

Ilya Serikov[1], Pablo Ristori[1], Martin Froidevaux[1], Todor Dinoev[1], Marian Taslakov[1], Valentin Simeonov[1], Yuri Arshinov[2], Sergei Bobrovnikov[2], Marc B. Parlange[1], Hubert Van den Bergh[1]

[1]Swiss Federal Institute of Technology, EPFL ENAC ISTE EFLUM, Station 2, CH-1015 Lausanne, Switzerland
E-mail: ilya.serikov@epfl.ch
[2]Institute for Atmospheric Optics, SB RAS, 1, Akademicheskii Ave., 634055, Tomsk, Russia, E-mail: arshinov@iao.ru

ABSTRACT

New temperature and water vapor Raman lidar operating in the solar blind region is presented. A multi-mirror telescope setup providing lidar signals with less than 2.5 dynamic range within the distance range 10 - 500 meters is described. Polychromators specially designed for the task of temperature and water vapor measurements with lidar are presented. The results from the first field experiment are demonstrated.

1. INTRODUCTION

To understand the interaction and feedback between the terrestrial ecosystem and the atmosphere, rapid (every few seconds) and spatially resolved (every few meters) vertical measurements of temperature and water vapor concentration in the atmospheric boundary layer are highly desired. We especially need measurements in the lower part of the boundary layer (up to several hundred meters), where the dynamics of the processes is the most strong. The Raman lidar technique appears to be most suitable for achieving the goal. Ro-vibrational Raman spectra of atmospheric water vapor, molecular nitrogen and oxygen together with the pure rotational Raman spectra (PRRS) of N_2 and O_2, excited by radiation of 266-nm wavelength are used to measure the moisture content [1] of the air and its temperature [2] respectively. The low efficiency of the Raman scattering as well as the high temporal and spatial resolution required for our measurements imply the use of the solar blind region (SBR) for water vapor detection. Even though the temperature measurements can be performed in the visible region if a Fabry-Perot interferometer is used to suppress the excessive daylight background [3] and despite the fact that isolating pure rotational Raman lines is easier at longer wavelengths, we decided to work with a single excitation at a wavelength in the SBR to simplify the lidar design. In addition, the time of a single temperature measurement was estimated to be from 10 to 100 times shorter, depending on the weather conditions, if working in the SBR.

2. LIDAR SETUP

The principle optical arrangement of the lidar is presented in Fig.1. The transmitter is based on a high-energy, high repetition frequency quadrupled Nd:YAG laser (Infinity 40-100).

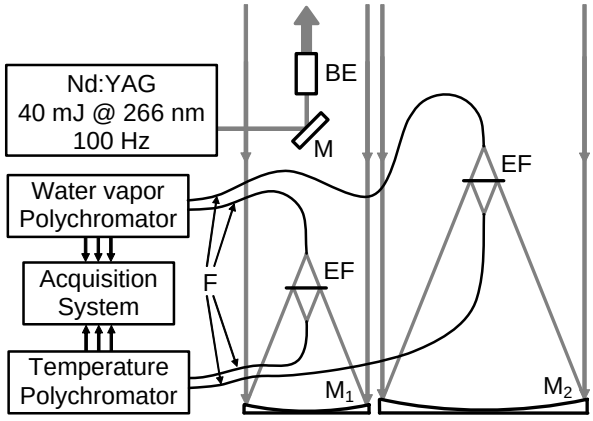

Fig.1 Optical arrangement of the lidar, where M is the folding mirror; BE - the beam expander M_1, M_2 – the parabolic mirrors of the co-axial and off-axial receiving telescopes, respectively; EF – the edge filters; F - the optical fibers.

The expanded laser beam is transmitted into the atmosphere, coaxially to one of the receiving telescopes. Steep edge filters (Barr Associates, Inc.), transmitting light at the wavelengths longer than 275 nm, and reflecting the shorter wavelengths separate PRRS from the ro-vibrational Raman spectra and block penetration of 266-nm radiation into the Raman-lidar channel of water vapor. Blocking 266-nm radiation at the entrance to fibers is essential for water vapor retrieval to avoid possible fluorescence in the fibers, which can interfere with the return signal from water vapor. Final spectral purity of the signals is achieved with the specially designed polychromators. The data acquisition system (Gage Applied Technologies Inc.) provides for fast digitizing of the lidar returns.

3. RECEIVING TELESCOPE

The power, P, of the backscattered light collected by a single-mirror telescope is proportional to its area A, to the overlap function of the lidar $G(r)$, and inversely proportional to the square of the distance to the scattering volume r

$$P \sim A\frac{G(r)}{r^2} = \frac{\pi}{4}\left(\frac{F}{F_{\#}}\right)^2 \frac{G(r)}{r^2}, \qquad (1)$$

where $F_{\#}$, is the telescope *f-number*. For a laser beam with the initial diameter d_0 and angular divergence γ, the diameter of the volume sounded at distance r from the lidar is $d_0+r\gamma$. As a first approximation, for $r>>F$, the image of the probe volume, produced by the receiving telescope, has a diameter $d_0\frac{F}{r}+F\gamma$. Intersection of the image forming light cone with a field-stop diaphragm (input end of the optical fiber in our case, Fig.1) yields the lidar overlap function $G(r)$. If the field stop diaphragm of the diameter d_{fs} is in the plane of the image of the probe volume located at distance $\hat{r}$, then for co-axial telescope configuration

$$G(\hat{r}) = \begin{cases} \left(\dfrac{d_{fs}}{d_0\dfrac{F}{\hat{r}}+F\gamma}\right)^2, & d_{fs} < d_0\dfrac{F}{\hat{r}}+F\gamma \\ 1, & d_{fs} \geq d_0\dfrac{F}{\hat{r}}+F\gamma \end{cases} \qquad (2)$$

Usually, the finite spectral pass band of a lidar channel (determined by a particular spectroscopic task), and the finite clear aperture of the system impose a limitation on the field-stop diameter and the f-number of the image-forming light cone, making a certain fixed value for the ratio of these two. In this case, the only free parameter of the telescope is its focal length, Eqs. 1-2. By increasing the focal length, we can increase the amount of collected light to the maximum value when the image size becomes equal to the field-stop diameter

$$d_{fs} = d_0\frac{F}{\hat{r}}+F\gamma \cdot \qquad (3)$$

Further increase of the focal length does not yield any signal growth, while an increase in the receiving area ($F_{\#}$ is fixed) is completely compensated for by the decrease in the fraction of light flux that goes through the field stop, Eqs. 1-3.

This simple model demonstrates that for each sounding distance there is an optimal focal length of the receiving telescope that allows one to collect the backscattered light with maximum efficiency. Following this idea, we have designed a multi-telescope lidar receiver that would enable us to minimize the dynamic range of the lidar signals, while keeping them at about maximum level within the operation range from 10 to 500 meters desired. Top view scheme of this four-mirror telescope assembly and the corresponding lidar returns simulated are shown in Fig.2. A small 10-cm-diameter telescope is coaxial with the laser beam and collects the lowest-range response. A 30-cm-diameter telescope collects light signal from the far range, while two 20-cm-diameter telescopes, being tilted at different angles with respect to the sounding beam, cover the middle range.

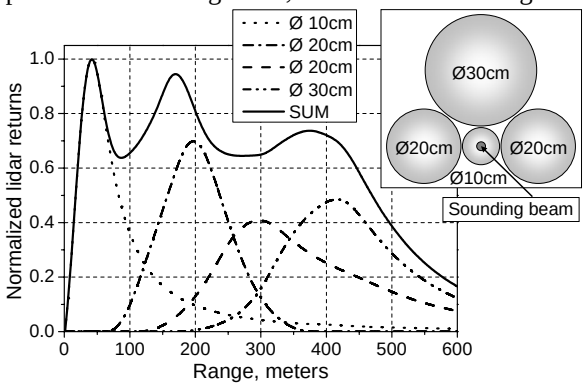

Fig.2 Simulated lidar returns for a multi-telescope setup.

Fig. 3 shows the lidar return due to elastic scattering acquired with the multi-telescope lidar receiver compared with the computer simulated one. The sum of returns presented in Fig.3 differs from that in Fig.2 because of the two times larger divergence of the sounding beam used in the experiment (Fig. 3).

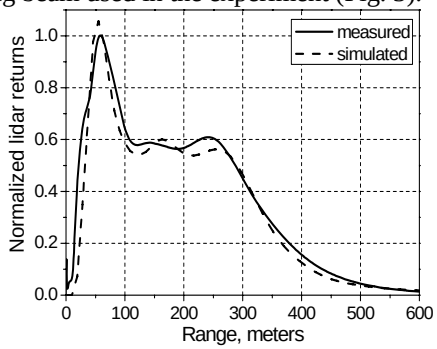

Fig.3 Measured and simulated lidar returns.

Good agreement between the measured and calculated returns, Fig.3, shows that the multi-telescope lidar, with the beam expander installed, should have a narrow dynamic range of the returns (about 2.5 within the range from 10 to 500 m, Fig.2), which gives nearly constant measurement accuracy within the operation range desired.

4. TEMPERATURE POLYCHROMATOR

A double stage diffraction grating polychromator, Fig.4, is used to isolate the temperature sensitive portions of the PRRS of the nitrogen and oxygen molecules.

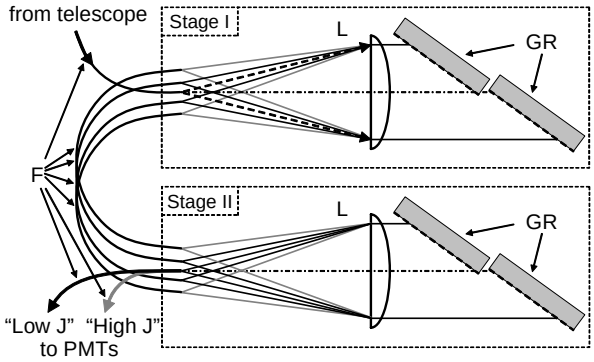

Fig.4 Optical layout of the temperature polychromator. F optical fibers; L lenses; GR diffraction gratings.

The principal idea of the polychromator is the same as presented in [4]. An optical fiber couples a single-mirror telescope with the first stage of the polychromator and plays the role of the polychromator entrance slit. The first stage of the polychromator produces, at its exit, four identical spectra (Out-1 to Out-4, in Fig.5) of light coming from the corresponding four fiber ends (In-1 to In-4) transporting light from the four telescopes of the lidar. Five optical fibers in each of the four spectra isolate the elastic line (central fiber) and other four portions of the PRRS. Then, in the Stage II of the polychromator, eight portions of the PRRS corresponding to low values of the rotational quantum number, J, are optically summed to form four output optical signals (Fig.5, right-hand panel) that are additionally summed on the photocathode of a PMT to produce the "low J" electrical signal at its anode. The same is done, in the Stage II of the polychromator, with the eight portions of the PRRS corresponding to high J values and another one PMT produces at its anode the "high J" electrical signal. It is just this range resolved profile of a ratio between these two electrical signals, which bears the information on the temperature profile along the sounding path.

To achieve the high linear dispersion needed to isolate the optimal lines of PRRS in the UV region we used a matrix of two diffraction gratings in both stages of the polychromator.

The narrow entrance slits (small diameter of the input fibers), high angular and linear dispersion of the polychromator, and the low level of parasitic stray light provided by the diffraction gratings (Richardson Gratings Lab) made it possible to isolate spectral lines with low rotational quantum numbers J (starting with J=2), which are highly sensitive to temperature. Working in the solar blind region with no daytime sky background allows one to isolate wider spectral portions of the PRRS and thus to increase the sensitivity of the temperature channel twice compared to what could be achieved in the visible region.

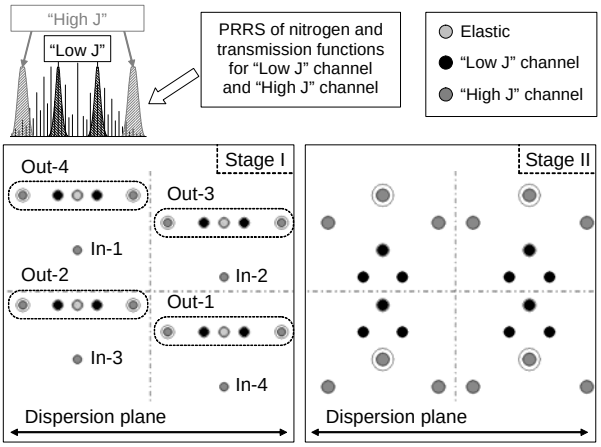

Fig.5 Scheme of input (In) and output (Out) fiber positions in the focal plane of the first and the second stages of the polychromator.

The high suppression of the elastic line in the Raman channels achieved with the polychromator (seven and eight orders of magnitude for the channels with low and high frequency shifts, respectively) allows temperature measurements to be performed even inside dense aerosol layers.

First data on daytime temperature (April 6th 2006, 10.06 UTC) acquired with the lidar operated along a horizontal path are presented in Fig.6.

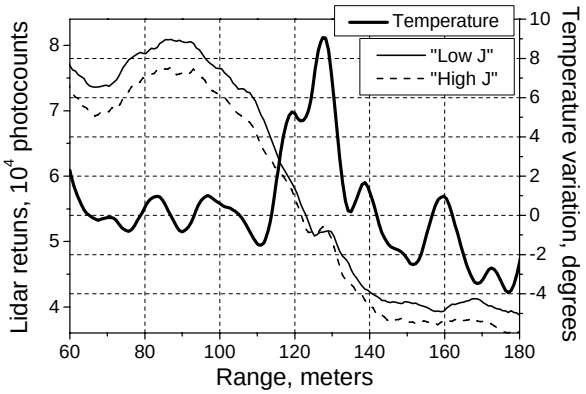

Fig. 6 Lidar returns and temperature profile. The range resolution is 4.5 meters, the averaging time is 27 seconds.

The effect of the propane torch installed below the laser beam at about 130 meters from the lidar is well pronounced on the lidar returns as well as on the temperature profile.

5. WATER VAPOR POLYCHROMATOR

To separate ro-vibrational Raman spectra of water vapor, nitrogen and oxygen molecules we use a prism polychromator shown in Fig.7. We have chosen prisms as a dispersion element because of the higher throughput, compared to diffraction gratings or interference filters, and the sufficient dispersion.

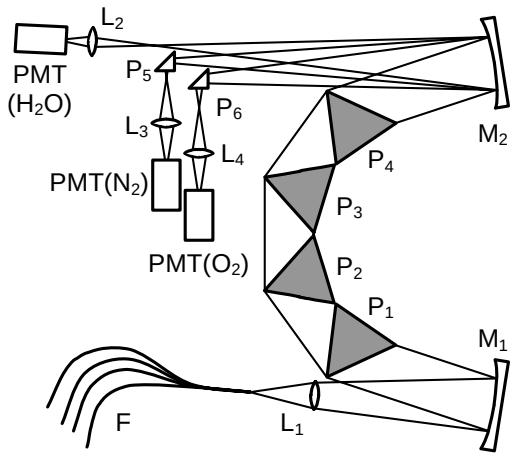

Fig.7 Optical arrangement of the polychromator, where F is a bundle of optical fibers; $L_1 – L_4$ are lenses; $M_1 – M_2$ mirrors; $P_1 – P_4$ dispersion prisms; $P_5 – P_6$ right-angle prisms.

The receiving telescope is coupled with the polychromator via the bundle of optical fibers. The fibers, arranged in a slit, form the entrance slit of the polychromator. The light is collimated with the lens L_1 and mirror M_1 then directed to the system of four dispersion prisms $P_1 – P_4$, which provides wavelength dependent angular separation. Being refocused by mirror M_2, the beam is spatially separated in three channels. Two right-angle prisms $P_5 – P_6$ are used to redirect the light to the PMTs in nitrogen and oxygen channels. Fourier transforming lenses ($L_2 – L_4$) installed in front of all PMTs provide the same position of the beam on the PMT photocathode for each fiber from the fiber bundle making the entrance slit.

The high purity of the dispersion prism material provides low level of parasitic scattered light in the polychromator, and hence, low crosstalk among the channels (better than 10^{-5}). The high throughput efficiency of the polychromator (better than 80%) allows accurate measurements with high spatial and temporal resolution. First daytime data acquired simultaneously with temperature measurements (Fig.6) is presented in Fig.8.

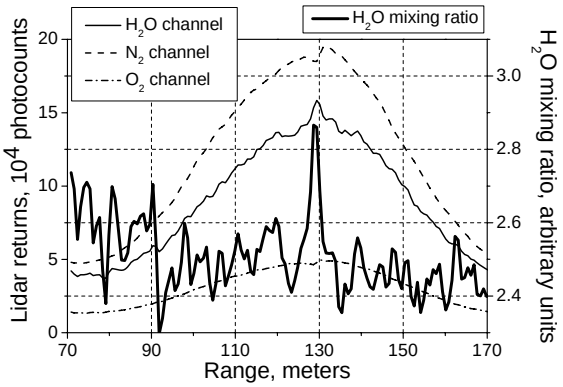

Fig. 8 Lidar returns and water vapor mixing ratio. April 6th 2006, 10.06 UTC. Range resolution - 1.5 meters, averaging time - 27 seconds.

A water vapor peak due to propane burning, well seen on the profile of the water vapor mixing ratio, is at the same distance as the temperature peak (Fig.6).

6. CONCLUSION

A multi-telescope configuration provides nearly constant signal from 10 to 500 meters, and therefore allows equal temporal and spatial resolution with constant measurement accuracy throughout the whole operational range. Field tests have demonstrated the capability of lidar to acquire temperature and moisture profiles with high spatial and temporal resolutions and quite reasonable accuracy. Further improvement of the system by decreasing the internal noise level of the ADC acquisition system is expected.

7. References

1. S.Melfi, J.Lawrence, M.McCormick, Observations of Raman scattering by water vapor in the atmosphere, Appl. Phys. Lett. 15, pp 295, 1969

2. J.A.Cooney, Measurement of atmospheric temperature profiles by Raman backscatter. J. Appl. Meteorology Vol.11, No.1, pp.108-112, 1972

3. Yu.Arshinov, S.Bobrovnikov, I.Serikov, A.Ansmann, U.Wandinger, D.Althausen, I.Mattis, D.Müller, Daytime operation of a pure rotational Raman lidar by use of a Fabry–Perot interferometer, Appl. Optics Vol.44, No 17, pp. 3593-3603, 2005

4. A.Ansmann, Yu.Arshinov, S.Bobrovnikov, I.Mattis, I.Serikov, U.Wandinger, Double grating monochromator for a pure rotational Raman-lidar, Proceedings of SPIE Vol. 3583, pp.491-497, 1998